Applied Catalysis B: Environmental 174–175 (2015) 376–382

Contents lists available at ScienceDirect

Applied Catalysis B: Environmental

journal homepage: www.elsevier.com/locate/apcatb

Accelerated bacterial reduction on Ag–TaN compared with Ag–ZrN and Ag–TiN surfaces

O. Baghriche[a,b], S. Rtimi[a], A. Zertal[b], C. Pulgarin[a,**], R. Sanjinés[c], J. Kiwi[a,*]

[a] Ecole Polytechnique Fédérale de Lausanne, EPFL-SB-ISIC-GPAO, Station 6, CH-1015 Lausanne, Switzerland
[b] Université Constantine1, Laboratoire des Techniques Innovants de Préservation de l'Environnement (LTIPE), Constantine 25017, Algeria
[c] Ecole Polytechnique Fédérale de Lausanne, EPFL-SB-IPMC-LPCM, CH-1015 Lausanne, Station 3, Switzerland

ARTICLE INFO

Article history:
Received 6 December 2014
Received in revised form 28 February 2015
Accepted 19 March 2015
Available online 20 March 2015

Keywords:
Ag–TaN composites
Co-sputtering
E. coli
Bacterial reduction
Redox catalysis
Photocatalysis
XPS
Ag-ionic sates

ABSTRACT

Ag–TaN sputtered on polyester (PES) accelerated >6 times the bacterial inactivation kinetics compared to TaN–PES under actinic light irradiation. Direct current pulsed magnetron sputtering (DCP) was used to sputter Ag–TaN–PES and TaN–PES. Complete bacterial reduction by Ag–TaN occurred within 20 min compared to Ag–TiN (100 min) and Ag–ZrN (90 min). The co-sputtering of Ag and Ta on PES was carried out in an Ar/N_2 10% atmosphere. By ion-coupled plasma mass-spectrometry (ICP–MS) a reduced Ag-release was observed for Ag–TaN samples compared to Ag–PES samples within the disinfection period. The redox catalysis by the Ag-species during the bacterial disinfection was followed by X-ray photoelectron spectroscopy (XPS). A bacterial reduction mechanism is suggested consistent with the experimental findings. The nitride films were characterized by surface science methods.

1. Introduction

Silver has been recognized as antibacterial agent in various material forms: colloids, powders and supported on natural textiles fibers like cotton and artificial fibers like polyester (PES). The silver ion-release kinetics, extended operational time and cytotoxicity (biocompatibility) determine its effective use when deposited on antibacterial surfaces [1,2]. There is at the present time a need to develop supported materials presenting fast bacterial reduction kinetics, substrate adherence, long-term operational lifetime, mechanical resistance and biocompatibility [3,4]. Nitrides and Ag-nitrides presenting fast kinetics seem to be ideal candidates for this task. Nitrides have been shown to be useful protective coatings due to their high thermal stability, hardness, mechanical resistance, chemical inertness, high electric resistivity and corrosion resistance.

Sol–gel methods have been used to graft TiO_2 and Ag thin films on substrates showing high thermal resistance. This method needs temperature of few hundred degrees to anneal the TiO_2 or Ag to the selected substrate. Sol–gel produced films are difficult to reproduce and exhibit low adhesion to the substrate. They lack uniformity and robustness making their practical application difficult [5].

We report in this study sputtered films of Ag–TaN prepared at temperatures below the PES temperature limit of 160 °C. Metal-nitride research is an area of increasing interest due to the nitride biocompatibility. Recent reports suggest that nitrides/oxynitrides do not induce any cellular changes being non-hemolytic or cytotoxic [6–8]. The gas composition Ar/N_2 has been shown to play a crucial effect on the microstructure of nitrides sputtered films [9–13]. Therefore, the optimization of the gas composition was systematically investigated during the film preparation. The amount of N_2 in the magnetron chamber gas phase controls the N- in the film improving the visible light absorption.

Synthetic antibiotics have been shown during the last decade to induce bacterial resistance when administered for long times [14–19]. For this reason we investigate in the present study the bacterial reduction by Ag–TaN nanoparticulate films. The bacterial reduction performance is presented for Ag–TaN and compared to Ag–TiN [20–25] and Ag–ZrN [26] films. The films prepared in our laboratory were performed under similar experimental conditions [20,26].

* Corresponding author. Tel.: +41 21 6936150; fax: +41 21 6935690.
** Corresponding author.
E-mail addresses: cesar.pulgarin@epfl.ch (C. Pulgarin), John.kiwi@epfl.ch (J. Kiwi).

http://dx.doi.org/10.1016/j.apcatb.2015.03.032
0926-3373/

Table 1
Surface composition of Ta and Ag on polyester/Ag–TaN found by X-ray fluorescence.

DCP	Time (*s*)	%Ag wt/wt	%Ta wt/wt	Thickness (nm)
Ag–TaN	5	0.0127	0.0030	6
300 mA/280 mA	10	0.0162	0.0076	12.5
	20	0.0250	0.0147	25
	40	0.0471	0.0227	50
	60	0.0605	0.0291	74
	120	0.0921	0.0487	150

We address in this study: (a) the preparation/optimization by DCP of Ag–TaN PES samples inducing a faster bacterial reduction kinetics compared to Ag–PES, (b) the co-sputtering details of TaN and Ag, being strongly dependent on the applied N_2 partial pressure, (c) the redox catalysis on Ag–TaN PES during bacterial reduction by X-ray photoelectron spectroscopy (XPS), (d) the Ag–TaN PES surface properties such as diffuse reflectance spectroscopy (DRS), X-ray fluorescence (XRF) and atomic force microscopy (AFM).

2. Experimental

2.1. Ag–TaN PES deposition by DCP co-sputtering techniques

TaN and Ag–TaN thin films were DCP sputtered simultaneously on PES using targets of Ag (99.99 at. %) and Ta (99.98 at. %) provided by K. Lesker, Hastings, UK. The substrate-to-target distance was 10 cm and the diameter of the targets was 5 cm. Before the deposition of the films the residual pressure in the sputtering chamber was fixed at 10^{-5} Pa. The total working pressure $P_{tot} = (P_{Ar} + P_{N2})$ was 0.5 Pa and the N_2 partial pressure in the Ar was 10%. The sputtering current on the Ta target was 280 mA providing a power of 100 W (U = −370 V) at a current density of 12.7 mA/cm^2. The sputtering current on the Ag target was 300 mA (P = 270 W, U = −400 V). Details regarding sputtering Ag have been recently reported [20,27].

The polyester used was Dacron, type 54 spun, plain weave ISO 105-F04 (EMPA) used for color fatness determinations. The thickness calibration of the Ag–TaN films and TaN was carried out on Si-wafers. The film thickness was determined with a profilometer (Alphastep500, TENCOR) and the values presented an error of ±10%.

2.2. Ag and Ta content, bacterial evaluation kinetics and irradiation procedures

The Ag- and Ta-content of PES were evaluated by X-ray fluorescence (XRF) in a PANalytical PW 2400 unit. The weight percentages of Ag and Ta in the Ag–TaN samples are shown in Table 1 as a function of the sputtering time. The optimal Ag–TaN photocatalyst (Ag–TaN co-sputtered for 20 s) had an Ag-content of 0.025 wt% Ag/wt PES and 0.0147 wt% Ta/wt PES.

The samples of *Escherichia coli* (*E. coli* K12) was obtained from the Deutsche Sammlung von Mikro-organismen und Zellkulturen GmbH (DSMZ) ATCC23716, Braunschweig, Germany to test the sample bacterial reduction activity. The PES was sterilized by autoclaving at 121 °C for 2 h. The 20 μL bacterial aliquots with a concentration ~10^6 CFU/mL^{-1} in NaCl/KCl were placed on the sputtered PES fabric. These samples were placed on Petri dishes provided with a lid to prevent evaporation. At preselected times the samples were transferred into a sterile 2 mL Eppendorf tube containing 1 mL autoclaved NaCl/KCl saline solution. These solutions were subsequently mixed thoroughly using a Vortex for 3 min. Serial dilutions were made in NaCl/KCl solution taking a 100 μL sample and then pipetting the aliquot onto a nutrient agar plate, for subsequent counting by the standard plate method. These agar plates were incubated, lid down, at 37 °C for 24 h before the colonies were counted. Triplicate runs were carried for the bacterial CFU/mL^{-1} determination reported in this study.

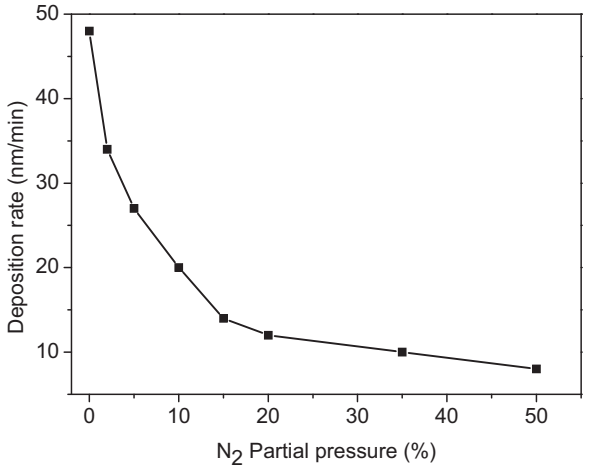

Fig. 1. Dependence of the deposition rate TaN films on the nitrogen partial pressure.

The samples used in the bacterial reduction were irradiated in the cavity of a L18 W/827 Lumilux/Osram reactor at different light doses.

2.3. Detection of released ions during bacterial reduction and optical absorption by the nano-particulate films

The Finnigan™ ICP–MS used was equipped with a double focusing reverse geometry mass spectrometer presenting an extremely low background signal and high ion-transmission coefficient. The spectral signal resolution was 1.2×10^5 cps/ppb and the detection limit of 0.2 ng/L. Diffuse reflectance spectroscopy was carried out using a PerkinElmer Lambda 900 UV–Vis–NIR spectrometer provided for with a PELA-1000 accessory

2.4. Atomic force microscopy and XPS studies

The AFM image signals were acquired in contact mode using a PSIA Xe-100 AFM. Silicon nitride cantilevers were used with feedback set points around 1.0 nN. The measurements in the z-scanner were not influenced by the hysteresis in the z-scanner.

$$R_a = \sqrt{\sum_{x,y}^{N} \frac{\left(Z_{x,y} - Z_{\text{average}}\right)^2}{N^2}}$$

An AXIS NOVA photoelectron spectrometer (Kratos Analytical, Manchester, UK) equipped with monochromatic AlKα (hν = 1486.6 eV) anode was used during the study. The carbon C1s position at 284.6 eV was the reference used to correct the charging effect. The XPS spectra were deconvoluted by means of the software CasaXPS-Vision 2, Kratos Analytical UK).

3. Results and Discussion

3.1. Thickness determination of sputtered polyester samples.

Fig. 1 shows the TaN film deposition rate as a function of the N_2 partial pressure in the DC-chamber. The deposition rate was 48 nm/min in the absence of N_2 for Ta films and decreased to <10 nm/min when 10% of N_2 gas was present in the Ar–N_2 gas mixture. This decrease is attributed to the blocking of Ta-target surface active sites by N-atoms at higher N_2 partial pressure [23,27]. The

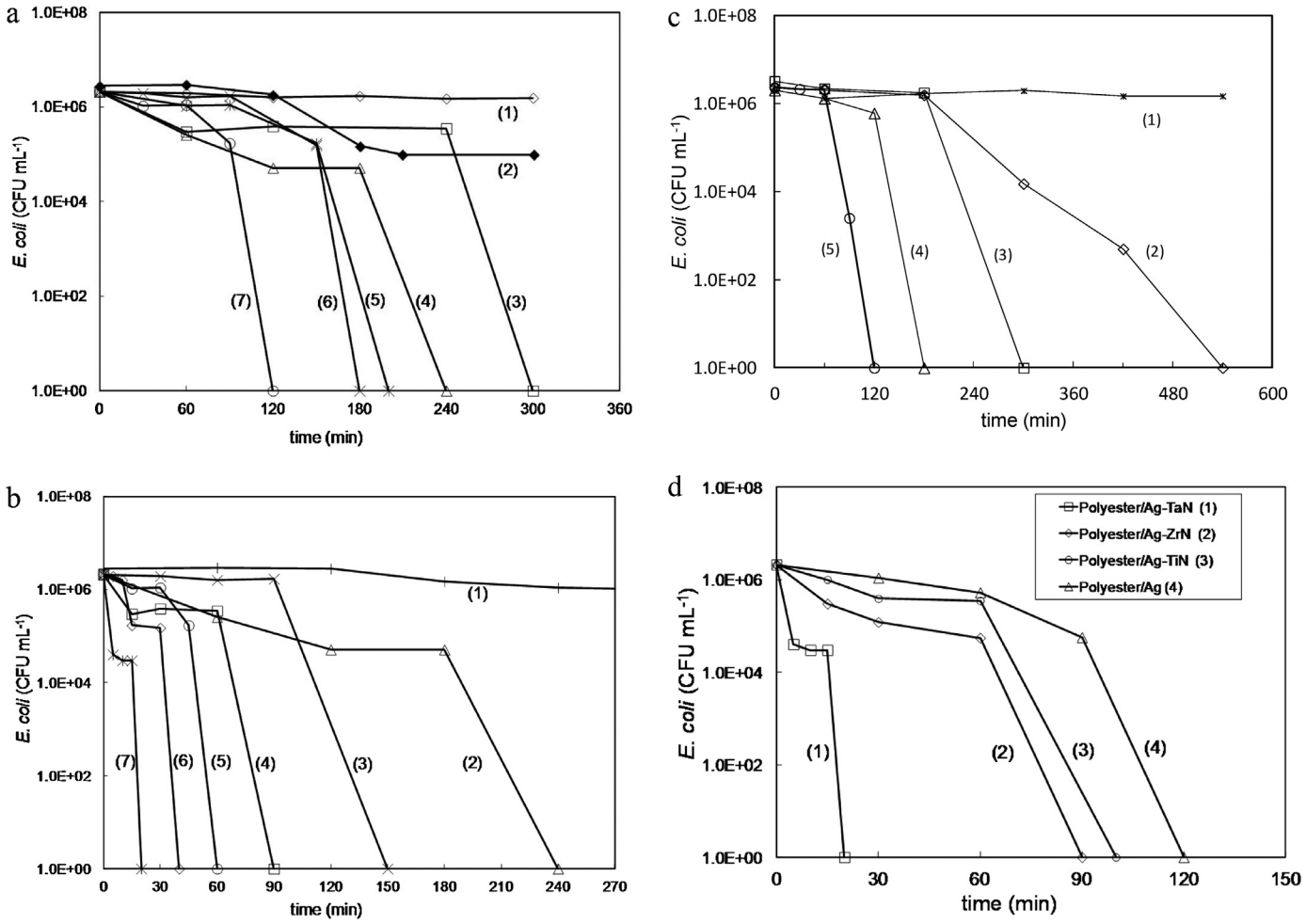

Fig. 2. (a). *E. coli* survival on TaN–PES in the dark and under light: (1) PES alone, (2) sputtered for 2 min in dark, (3) sputtered for 1/2 min under light, (4) sputtered for 1 min under light, (5) sputtered for 8 min under light (6) sputtered for 4 min under light and (7) sputtered for 2 min under light. Irradiation source L18 W/827 Lumilux/Osram(4 mW/cm^2 (b). *E. coli* bacterial reduction on Ag–TaN sputtered for times: (1) PES, (2) for 5 s, (3) for 10 s, (7) for 20 s, (6) for 40 s, (5) for 60 s and (4) for 120 s. Irradiation source L18 W/827 Lumilux/Osram (4) mW/cm^2). (c). *E. coli* bacterial reduction on Ag-sputtered (1) PES alone, (2) for 20 s, (3) for 40 s, (4) for 80 s and (5) for 160 s. Irradiation source L18W/827 Lumilux/Osram (4 mW/cm^2). (d). Comparative bacterial reduction kinetics of *E. coli* on: (1) Ag–TaN PES, (2) Ag–ZrN PES (3)Ag–TiNPES, and (4) Ag–PES.

N-content has been reported to increase up to Ta_3N_5 [24] during the sputtering of TaN.

Table 1 shows that the mass of Ag and Ta deposited on PES are not directly proportional with the time of sputtering meaning that the composition of the film changes with sputtering time. More dense layers predominate at shorter deposition times. At longer sputtering times, due to the lower amounts added of Ag and Ta as shown in Table 1 these layers became less dense. The thicknesses of the TaN and Ag–TaN layers were observed to be a function of the sputtering time on Si-wafers. Table 1 shows that the layer thickness is directly proportional to the sputtering time. Within 1 s, an Ag layer of 1.2–1.25 nm Ag was deposited on PES equivalent to ~6 atomic layers of 0.2 nm each, at a rate of 6×10^{15} atoms/cm^{2}xs. If a lattice distance of 0.3 nm is assigned between Ag–atoms [8], a layer consists of 10^{15} atoms/layer/cm^2. Being each layer 0.2 nm thick, a TaN layer 400 nm thick would contain 2×10^{18} atoms/cm^2, deposited at a rate of 2×10^{15} atoms/cm^2 x s.

3.2. *E. coli* bacterial reduction by TaN–PES and Ag–TaN PES

Fig. 2a presents the *E. coli* reduction kinetics when Ta was sputtered on PES in an Ar + N_2 (0.5 Pa) atmosphere for different times. Fig. 2a shows the semiconductor behavior of the Ta sputtered on PES. The TaN PES sample sputtered for 2 min under light led to complete bacterial reduction within 120 min (Fig. 2a, trace 7).

The formation of Ta_2O_5 is possible during the sputtering of TaN in the magnetron chamber since: (a) residual H_2O vapor is present in the sputtering cavity at $Pr = 10^{-4}$ Pa. This pressure is equivalent to 10^{15} molecules/cm^{2}s or one monolayer and the O-radicals produced induce Ta partial oxidation and (b) the TaN films can also oxidize after the deposition when exposed to air and during the sterilization process used during the bacterial counting autoclaving at 121 °C.

Fig. 2a shows that the bacterial reduction kinetics on TaN–PES sputtered for 0.5–2 min (Fig. 2a, traces 3, 4, 7). Fig. 2a, traces 5,6 sputtered for 8 and 4 min, respectively, show slower bacterial inactivation kinetics compared to trace 7 (2 min). This is due to the increase in the TaN layer thickness leading to bulk inward diffusion of the charge carriers induced by light irradiation [28].

Fig. 2b shows the faster bacterial reduction of *E. coli* on Ag–TaN PES surfaces under a Lumilux/Osram L18 W/827 lamp irradiation. It is readily seen that PES alone has no bactericide action and that the *E. coli* reduction kinetics becomes faster at longer Ta/Ag co-sputtering times up to 20 s. This sample led to a complete bacterial reduction within 20 min. Sputtering times > 20 s led to a slower bacterial reduction kinetics. For a sample sputtered for 120 s (see Fig. 2b, trace 4) the *E. coli* bacterial reduction became longer since

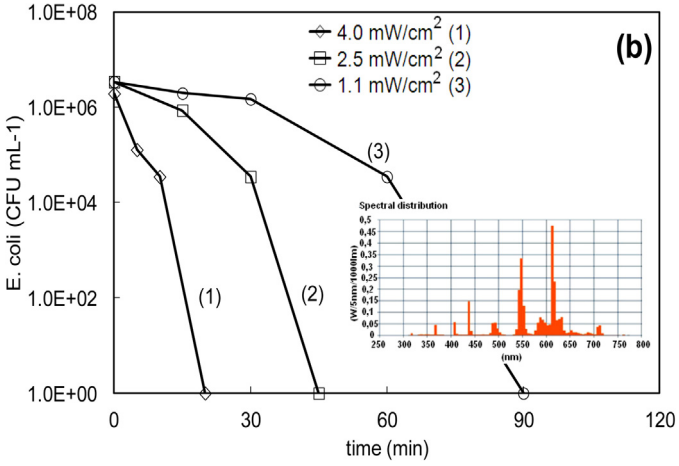

Fig. 3. *E. coli* bacterial reduction kinetics on Ag–TaN PES cosputtered for 20 s on polyester as a function of the applied light dose. Irradiation source L18 W/827 Lumilux/Osram (4 mW/cm^2).

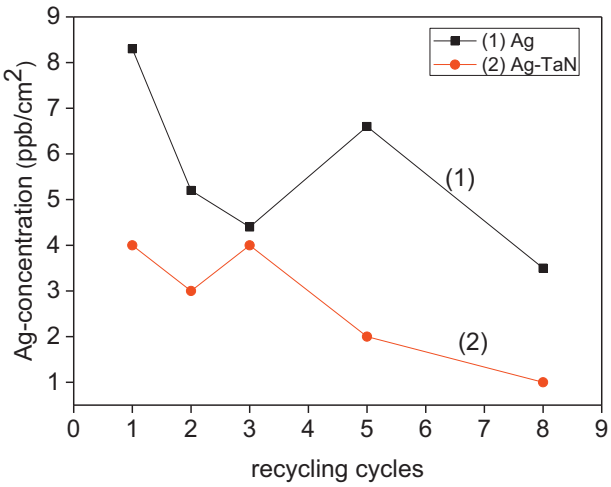

Fig. 4. (a) Ion-coupled plasma spectrometry (ICP–MS) determination of Ag-ions released during the recycling of (1) Ag–PES sputtered for 160 s and (2) Ag–TaN PES co-sputtered for 20 s.

the Ag-clusters size agglomerated, reducing the catalytic activity per exposed Ag-atom.

Fig. 2c shows the *E. coli* survival on Ag–PES. Sputtering of Ag for 160 s induced the fastest bacterial reduction in Fig. 2c, trace 5. The sputtering time of 160 s seems to lead to the optimal ratio of Ag-loading/Ag-cluster size with the highest amount of Ag-sites held in exposed positions on the PES-surface.

A drastic acceleration of the bacterial reduction kinetics is observed in Fig. 2b compared to Fig. 2a. It has been suggested that during the sputtering of nitrides on PES, the bonding of the TaN adatoms proceeds with a high alignment on the PES and this has an effect on the added Ag. It has been reported that the atoms of the nitride film merge without forming boundaries leading to a smooth uniform nitride surface [8–10]. The significant effect of TaN on the Ag compared to Ag–ZrN and Ag–TiN on the bacterial reduction is shown in Fig. 2d. The 20 min bacterial reduction time represents a drastic bacterial reduction time compared with Ag–TiN within 100 min [20] and Ag–ZrN within 90 min [26] under similar experimental conditions. In Fig. 2d, the initial induction period during the bacterial reduction was around 60 min for Ag–TiN and Ag–ZrN while it was only 15 min for Ag–TaN.

To find an explanation for the shorter bacterial reduction on Ag–TaN, (Ta^{5+} 0.73A) compared to Ag–TiN (Ti^{4+} 0.64A) and Ag–ZrN (Zr^{4+} 0.87A) is not possible based on the size of the cations. Due to the similar radii, it is possible to discard nitride cation size considerations to rationalize the observed effect. But there is a significant difference in the potentials of TaN undergoing Ta^{5+}/Ta^{6+} redox reactions compared to TiN and ZrN undergoing M^{3+}/M^{4+} redox reactions [23–34,29]. The oxidation-reduction potential values for the Ta, Ti and Zr depend heavily on the nature of the composite compound they are found. To provide an explanation based on the cations potentials is not possible at the present time since the exact state of the Ta, Ti and Zr in the nitrides has not been reported.

3.3. Effect of the applied light dose and suggested mechanism of reaction

Fig. 3 presents the bacterial inactivation kinetics mediated by Ag–TaN PES (20 s) applying different light doses. The bacterial inactivation kinetics in Fig. 3 is seen to be dependent on the applied light dose. A dependence on the light dose reveals semiconductor behavior inducing charge separation in Ag_2O. At the highest light dose in Fig. 3, the induction period is negligible and bacterial reduction starts immediately after the sample irradiation.

The bacterial inactivation kinetics of *E. coli* on the Ag–TaN (20 s) samples was evaluated for CFU initial concentrations of 1.8×10^6, 1.5×10^7 and 1.47×10^9 CFU/mL^{-1}. The inactivation of higher bacterial concentrations required longer times. This observation excludes a strong absorption of *E. coli* K12 on the co-sputtered Ag–TaN (20 s) sample. Adsorption of *E. coli* on the 30 nm Ag-particles is not possible due to the size of *E. coli* K12 (1 μ) [30].

3.4. Repetitive bacterial reduction and Ag-release during bacterial reduction.

The cyclic bacterial reduction by Ag–TaN PES (20 s sputtered sample) was carried out under light up to 8 cycles. After each cycle, the sputtered polyester fabrics were washed thoroughly with sterilized MQ-water, vortexed for 3 min and dried. No bacteria were detected on the polyester fabric. To verify that no re-growth of *E. coli* occurs after the first bacterial reduction cycle, the TaN–Ag nanoparticle film was incubated again on an agar Petri dish at 37 °C for 24 h. No bacterial re-growth was observed.

During the repetitive cycling runs the complete bacterial reduction increases from ~20 min in the first cycle reaching in the 8th cycle ~35 min. The possible Ag-losses during the bacterial reduction may account for the longer bacterial reduction time observed during the repetitive bacterial reduction cycles (data not shown). This moved us to evaluate the Ag-release by ICP–MS.

The release Ag from Ag–PES (160 s) and Ag–TaN PES (20 s) is shown in Fig. 4 up to the 8th recycling. For the Ag–PES samples, the level of Ag-release drops from 8 to about 4 ppb/cm^2 after the 8th cycle. For the Ag–TaN (20 s) sample, the Ag-release drops from 4 to about 1 ppb/cm^2. Ag-ions > 0.1 ppb present antimicrobial effects and Ag > 35 ppb become cytotoxic to human (mammalian) cells [31,32]. Ag-ions due to their small size are able enter the 1.0–1.1 nm porins channels of *E. coli* and penetrated into the bacterial cytoplasm [30,33,34].

Silver bioactivity does not involve exclusively Ag ion-release. Other bioactive mechanisms are present during the direct contact between Ag- and pathogens intervening in the bacterial reduction [16,18,32].

3.5. Diffuse reflectance spectroscopy (DRS) and visual perception of samples.

The DRS spectra of Ag–TaN PES surfaces increase as a function of Ag-sputtering time ~400 nm (data nor shown). Ag-plasmons have

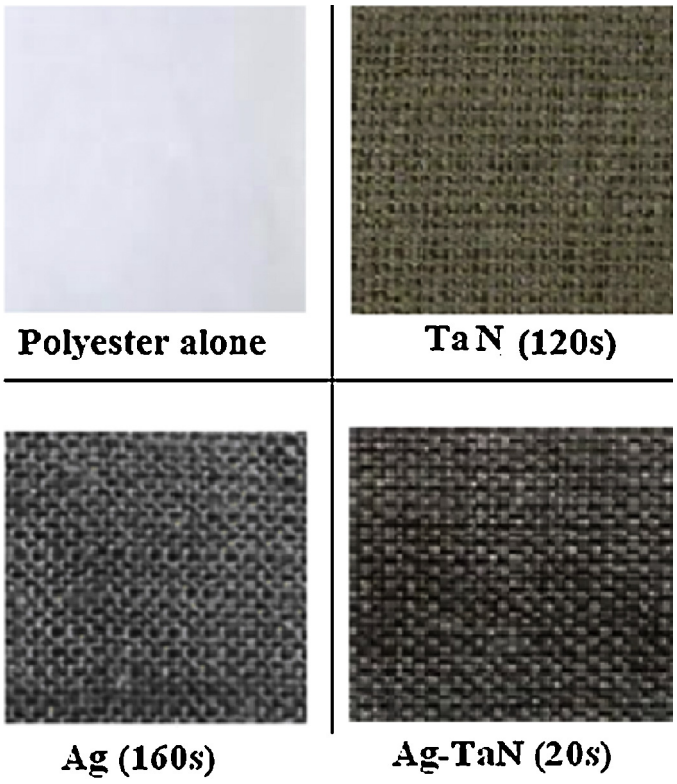

Fig. 5. TaN, Ag and Ag–TaNsputtered PES for different times noted in the figure. For other details see text.

been reported on different surfaces [9–10]. The UV–vis reflectance data cannot be used directly to assess the absorption coefficient because of the large scattering contribution to the DRS spectra. At a higher Ag-concentration >20 s sputtering time (see Table 1), the Ag acts as a carrier recombination center. No clear XRD metallic Ag signals were obtained for Ag on PES due to the low amount of Ag-sputtered on PES.

The visual perception of sputtered samples is shown in Fig. 5. PES alone is white but when sputtered with TaN for 2 min it becomes brown. Sputtering Ag for 20 s led to a dark gray color PES samples that became black when the Ag was co-sputtered with TaN for 20 s. The dark gray color corresponds to the Ag_2O with a 0.7–1.0 eV band-gap presenting an absorption up to ~1000 nm [20]. When AgO clusters/films are exposed to air, the H_2O vapor in the air transforms this silver in AgOH. But AgOH is not stable and follows the

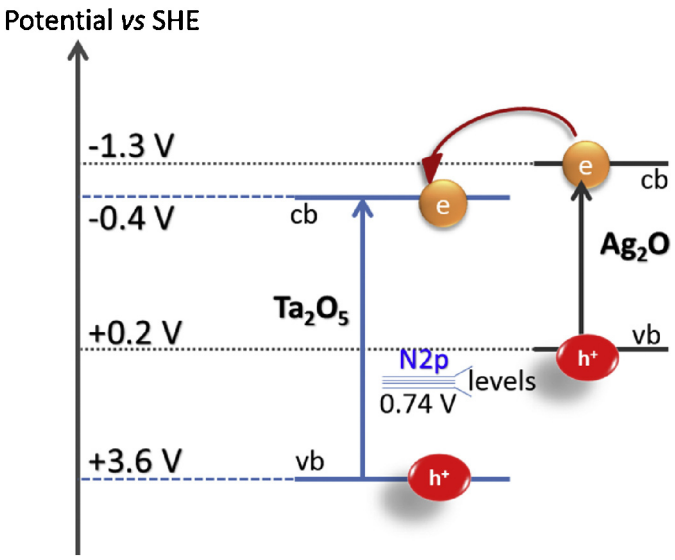

Fig. 6. Transmission electron microscopy (TEM) of: (a) TaN–PES sputtered for 2 min and (b) Ag–TaN co-sputtered for 20 s on PES.

lowest energy path and spontaneously decomposes to Ag_2O and H_2O [8].

Fig. 6 shows the scheme for the electron injection under actinic light from Ag_2O to Ta_2O_5. The Ag_2O electronic band positions: cb at −1.3 eV NHE (pH 0), vb at +0.2 V NHE (pH 0) and the band-gap (bg) of 1.5 eV have been reported [29]. The wide band-gap semiconductor Ta_2O_5 has been reported presenting a cb at −0.4 V, vb at +3.6 V NHE (pH 0) and a band-gap of 4.0 eV. The electron injection from Ag_2O to the TaN intermediate lower lying band states located at 0.74 V above the Ta_2O_5 vb is shown in Fig. 6 [35]. The Ag_2Ocb electrons injected into Ta_2O_5cb hinder the e^-/h^+ recombination in Ag_2O. These injected electrons enhance the O_2–O_2^- reduction since Ta_2O_5cb (−0.4 eV) potential is situated well below the Ag_2Ocb (−1.3 eV). Under light irradiation Ag_2O generate the charges:

$$R_a = \sqrt{\sum_{x,y}^{N} \frac{\left(Z_{x,y} - Z_{\text{average}}\right)^2}{N^2}} \quad (1)$$

$$Ag_2O + h\gamma \rightarrow h^+ + e^- \quad (2)$$

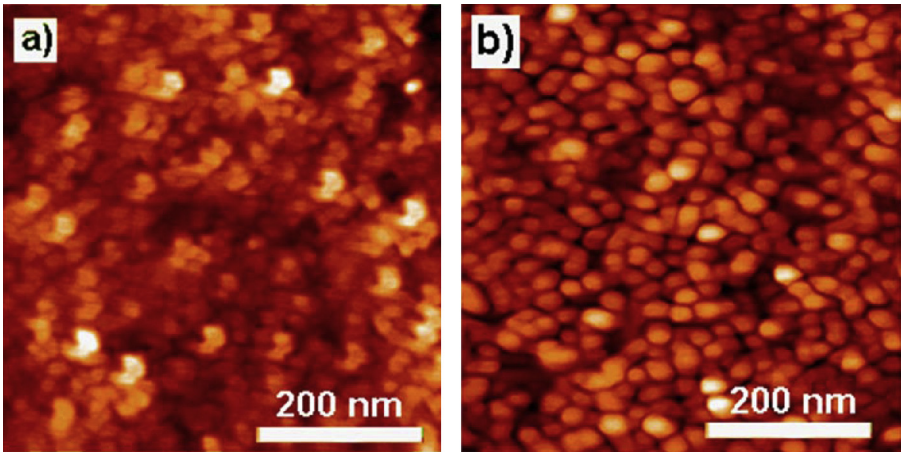

Fig. 7. Atomic force microscopy for Si-wafers: (a) sputtered with TaN for 120 s and (b) cosputtered for 20 s Ag–TaN.

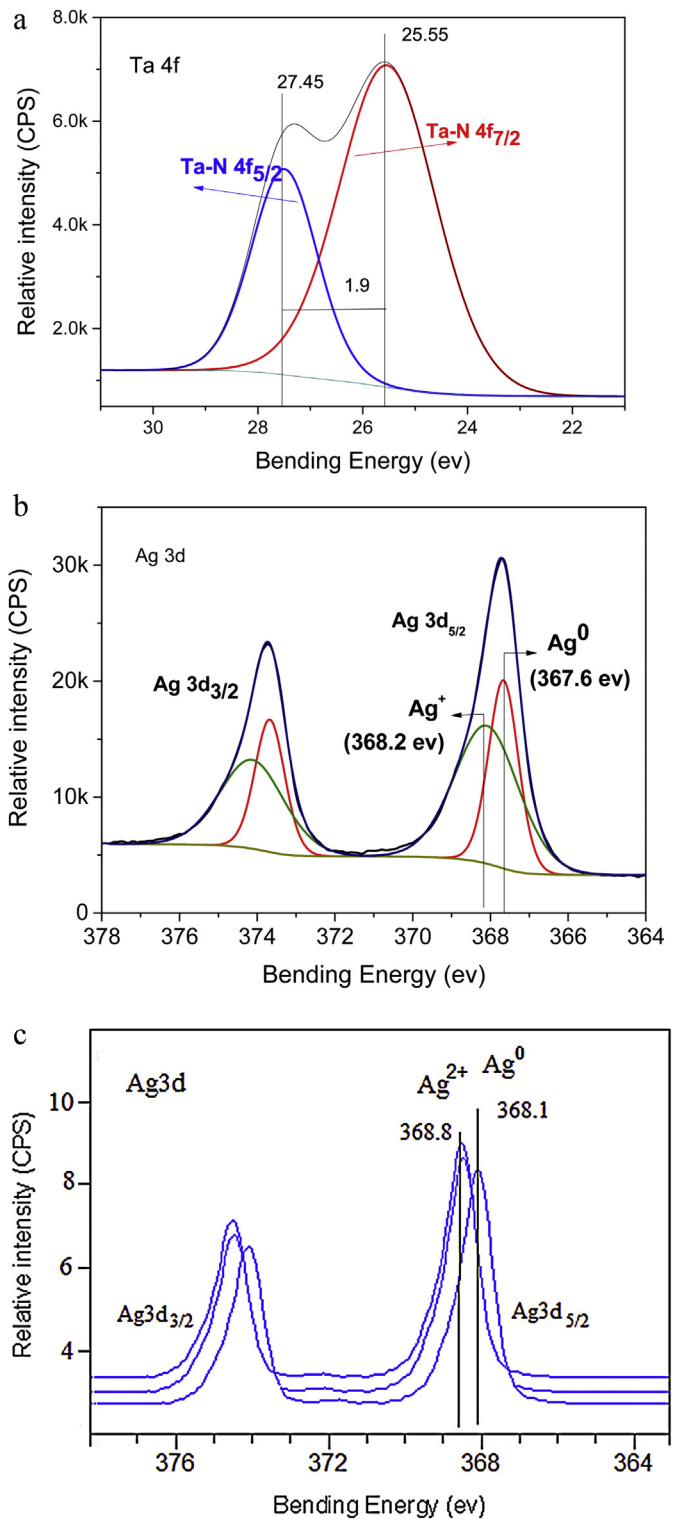

Fig. 8. (a). XPS found for the Ta4f$_{2/5}$ doublet for TaNsputtered PES for 2 min. (b). XPS of the Ag3d5/2 doublet at time zero on Ag–TaN sputtered PES for 160 s. (c). XPS Ag3d5/2 doublet for Ag–TaN sputtered PES for 20 s after 20 min bacterial reduction under a L18 W/827 Lumilux/Osram (4 mW/cm^2)actinic irradiation source.

The electron in Eq. (2) will also reduce O_2 leading to O_2^- Eq. (3) and in the presence of water vapor leads to highly oxidative radicals OH° able to reduce bacteria as shown in Eq. (4)

$$e^- + O_2 \rightarrow O_2^- \quad (3)$$

$$e^- + H_2O + 1/2O_2 \rightarrow O\,H^{\bullet} + O\,H^- \quad (4)$$

3.6. Atomic force microscopy (AFM)

Fig. 7a presents the atomic force microscopy (AFM) for a sputtered TaN (2 min) with TaN grain sizes of 30–50 nm. Fig. 7b shows image for co-sputtered samples of Ag–TaN (20 s) with grain sizes of 70–100 nm. The surface roughness of the samples was evaluated by the root mean square (rms) for TaN and Ag–TaN and attained values of 2.2 and 2.7 nm. An increase in roughness leads to a higher contact angle reducing the polarity and the surface energy. Increase in the surface roughness generally leads to a better contact of the Ag, and has a beneficial effect accelerating the bacterial reduction kinetics. The Rg values found were in the range of low surface roughness (<3 nm). In this range it is unlikely that the roughness variation between the samples have a significant effect on the contact angle measurements for TaN–PES and Ag–TaN PES. The nanoparticles in the AFM-image (Fig. 7) appear separated from each other showing a large contrast along the z-axis. This suggests a low uniformity for the coverage shown in Fig. 7a,b.

3.7. Photoelectron spectroscopy (XPS) of the Ag–TaN PES

The results in Fig. 8a–c show the XPS deconvolution of TaN and Ag-peaks found by XPS and provide information on the Ag-ionic states on the Ag–TaN PES. Fig. 8a presents the TaN PES sputtered for 2 min as it led to the fastest bacterial inactivation (Fig. 2a). The core line is centered at 25.55 eV for Ta 4f$_{2/5}$ and the spin orbit separation was 1.9 eV, indicating the presence of Ta^{5+} [36]. A lower valence state of Ta could not be detected because of the PES coverage of Ag and its possible low surface concentration. The observed ratios of Ta/Ag and O/N were 2.43 and 1.03, respectively. These XPS results indicate that besides Ta, O adsorbed from the air is found in the topmost layers of Ag–TaN PES.

The XPS of the Ag on the Ag–TaN PES sputtered for 160 s is shown next in Fig. 8b for Ag°/Ag^+ peaks and Ag^0/Ag^{2+}peak, respectively. Ag_2O (Ag^+) and AgO (Ag^{2+}) species were detected by XPS due to the oxidation of Ag by air on PES. The Ag° metal state signal still persists along the Ag-ionic states as shown in Fig. 8b. The electrostatic correction for the XPS Ag-signals was carried out according to Shirley [37]. Fig. 8b shows at time zero the Ag3d$_{5/2}$ doublet with Ag° at 367.6 eV and the Ag^+ doublet at 368.2 eV.

Fig. 8c shows that after 20 min bacterial reduction, the Ag^0 doublet shifts to 368.8 eV and a new signal appears for the Ag^{2+} doublet appears at 368.8 eV. Redox processes take place involving Ag-ionic states during the bacterial reduction. These redox processes involve charge transfer between the Ag–TaN leading to *E. coli oxidation.* A shift in the XPS binding energy (BE) >0.2 is the evidence for a shift in the metal oxidation state occurring during bacterial reduction [38].

4. Conclusions

TaN induces a drastic acceleration on the Ag bacterial reduction when compared to TiN and ZrN matrices. Ag-redox changes were identified by XPS during the bacterial reduction process. Evidence was found by ICP–MS for the Ag–TaN PES slowing the Ag-release during *E. coli* compared to Ag–PES. A mechanism for the bacterial inactivation by Ag–TaN is suggested in this study.

Acknowledgments

We thank the EPFL, the Swiss National Science Foundation (SNF) Project (200021-143283/1) and the EC7th Limpid FP project (Grant No 3101177) for financial support. We also thank the COST Action NMP 1106 for interactive discussions during the course of this study.

References

[1] I. Sondi, S.J. Sondi, Coll. Interf. Sci. 275 (2006) 177–182.
[2] J. Liu, D. Sonshine, S. Shervani, R. Hurt, ACS Nano 4 (2010) 6903–6913.
[3] S. Dancer, J. Hosp. Infect. 73 (2009) 378–386.
[4] I. Kramer, I. Schwebke, G. Kampf, Diseases 6 (2006) 137–146.
[5] L. Zhang, R. Dillert, D. Bahnemann, M. Vormoor, Energy Environ. Sci. 5 (2012) 7491–7507.
[6] J. Probst, U. Gbureck, R. Thull, Binary Surf. Coat. Technol. 148 (2001) 226–233.
[7] F. Magnus, O. Sveinsson, S. Olafson, J. Gudmundsson, J. Appl. Phys. 110 (2011) 083306.
[8] P.A. Ehiasarian, A.Y. Gonzalvo, D.T. Whitmore, Polymers 4 (2007) 5309–5313.
[9] K. Sarakinos, J. Alami, S. Konstantinidis, Surf. Coat. Technol. 204 (2010) 1661–1684.
[10] J. Lin, J. Moore, W. Sproul, W. Mishra, W. Wang, Surf. Coat. Technol. 2014 (2010) 2230–2239.
[11] B.A. Pinaud, A. Vailionis, T.F. Jaramillo, Chem. Mater. 26 (2014) 1576–1582.
[12] S. Rtimi, O. Baghriche, R. Sanjines, C. Pulgarin, M. Ben-Simon, J.-C. Lavanchy, J. Kiwi, J. Photochem. Photobiol. A 256 (2013) 52–63.
[13] Epitaxial growth. J. Part B, in: W. Mathews (Ed.), Nucleation of Thin Films, Academic Press, New York, 1975, pp. 382–486, Ch 4.
[14] G. Borkow, J. Gabbay, Cur. Chem. Biol. 3 (2009) 272.
[15] K. Page, M. Wilson, I.P. Parkin, J. Mater. Chem. 19 (2009) 3819–3831.
[16] D. Cazzoli, E. Fanizza, R. Comparelli, L. Currri, A. Agostiano, J. Phys. Chem. B 108 (2004) 9623–9630.
[17] A. Fujishima, X. Zhang, D. Tryck, Surf. Sci. Rep. 63 (2008) 515–582.
[18] K. Vasilev, J. Cook, H. Griesser, Expert Rev. Med. Devices 6 (2009) 553–567.
[19] K.M. Seery, R. George, P. Floris, S.C. Pillai, J. Photochem. Photobiol. A 189 (2007) 258–263.
[20] S. Rtimi, O. Baghriche, R. Sanjines, C. Pulgarin, M. Ben-Simon, J.-C. Lavanchy, A. Houas, J. Kiwi, J. Appl. Catal. B 123–124 (2012) 306–315.
[21] P. Kelly, H. Li, P. Benson, K. Whitehead, J. Verran, R. Arnell, I. Iordanova, Surf. Coat. Technol. 205 (2010) 1606–1610.
[22] P. Kelly, H. Li, K. Whitehead, J. Verran, R. Arnell, I. Iordanova, Surf. Coat. Technol. 2014 (2009) 1137–1141.
[23] L. Wan, J. Li, J. Feng, W. Sun, Z. Mao, Appl. Surf. Sci. 253 (2007) 4764–4767.
[24] J.-M. Chappé, N. Martin, J. Lintymer, F. Stahl, G. Terwagne, J. Takadoum, Appl. Surf. Sci. 253 (2005) 5312–5316.
[25] Z. Kertzman, J. Marchal, M. Suarez, P.M. Staia, P. Filip, S. Kohli, J. Aouadi, Biomed. Mater. Res. 84 (2008) 1061–1067.
[26] O. Baghriche, J. Kiwi, C. Pulgarin, R. Sanjines, J. Photochem. Photobiol. A 229 (2012) 39–45.
[27] C. Geetha, A. Sebareeswaran, P. Mohanan, Toxicol. Mech. Methods 22 (2012) 144–150.
[28] Y. Jeyachandran, S. Narayandas, Trends Biomater. Artif. Organs 24 (2010) 90–93.
[29] A. Nozik, Photo-effects at the semiconductor electrolyte interface, in: ACS Symp. Ser. 140. Amer. Chem. Soc, Washington, 1990.
[30] H. Nikaido, J. Biol. Chem. 269 (1994) 3905–3909.
[31] O. Bondarenko, K. Juganson, A. Ivask, K. Kasemets, M. Mortimer, A. Kahru, Crit. Rev. Arch. Toxic. 87 (2013) 1181–2000.
[32] H. Foster, I. Ditta, S. Varghese, A. Steele, Appl. Microbiol. Biotechnol. 90 (2012) 1847–1868.
[33] M. Radzig, V. Nadtochenko, O. Koksharova, J. Kiwi, V. Lipasova, I. Khmel, Colloids Surf. B Bio-Interfaces 102 (2013) 300–306.
[34] X. Li, H. Nikaido, K. Williams, J. Bacteriol. 179 (1997) 6127–6132.
[35] S. Banerjee, S.C. Pillai, P. Falaras, K.E. O'shea, J.A. Byrne, D. Dionysiou, J. Phys. Chem. Lett. 5 (2014) 2543–2555.
[36] Handbook of X-Ray photoelectron spectroscopy, in: C.D. Wagner, M. Riggs, E.L. Davis, G.E. Müllenberg (Eds.), PerkinElmer Corporation Physical Electronics Division, Minnesota, 1979, 2015.
[37] A.D. Shirley, Corrections of Electrostatic Charged Species in XSP-Spectroscopy, Physi. Rev. B5 (1972) 4709–4716.
[38] J. Nogier, M. Delamar, P. Ruiz, M. Gratzel, R. Thampi, J. Kiwi, X-Ray Cat. Today 20 (1994) 109–123.